Nonlinear Fiber Transmission of Compressed Shaping Signals

Tsuyoshi Yoshida[(1,2)], Takashi Inoue[(3)], Koji Igarashi[(2)], Masashi Binkai[(1)],
Yoshiaki Konishi[(1)], Naoki Suzuki[(1)], Magnus Karlsson[(4)], and Erik Agrell[(4)]

[(1)] IT R&D Center, Mitsubishi Electric Corporation, Yoshida.Tsuyoshi@ah.MitsubishiElectric.co.jp
[(2)] Graduate School of Engineering, Osaka University
[(3)] National Institute of Advanced Industrial Science and Technology (AIST)
[(4)] Fiber Optic Communications Research Center (FORCE), Chalmers University of Technology

Abstract *In nonlinear transmission of compressed shaping signals, the optimum launch power decreases as source entropy decreases, but the maximum Q performance based on soft information increases for either bit-interleaved coded or multilevel coded modulation. The excess degradation is mostly recovered by high-performance multi-channel nonlinearity compensation. ©2022 The Author(s)*

Introduction

For supporting continuously growing traffic demands, highly efficient fiber-optic transmission techniques are required. Coherent systems with digital signal processing (DSP) [1] have been widely deployed in transponders for short to ultra-long-haul applications [2]. Channel coding, e.g., multilevel modulation, forward error correction (FEC) [3,4], and probabilistic constellation shaping (PCS) [5,6], can efficiently close the gap to the Shannon capacity depending on the signal-to-noise ratio (SNR).

To improve the performance beyond what pure PCS enables, a joint source–channel coding scheme called compressed shaping was proposed in [7,8]. In this technique, the conventional assumption of uniformity in the source-bit probability mass function given by full bit-scrambling before channel coding is relaxed. Instead, the source nonuniformity caused by sparse user traffic is exploited for reducing the channel-input symbol entropy. Compressed shaping requires a smaller SNR than conventional PCS for a given information rate with an FEC over additive white Gaussian noise (AWGN) channels.

In this work, the fiber transmission performance of compressed shaping is studied, for the first time to our knowledge, with a base constellation of 64-ary quadrature amplitude modulation (QAM). The power consumption in the soft-decision (SD) FEC decoding and the influence of nonlinearity compensation (NLC) using a recently developed learning-based digital back propagation (LDBP) scheme [9] in compressed shaping are also investigated.

System model and simulation conditions

Fig. 1 shows the system model with compressed shaping and its frame structure for coded modulation, where S denotes a random source bit and X a random channel-input symbol. The smaller the source bit entropy $\mathbb{H}(S)$, the smaller
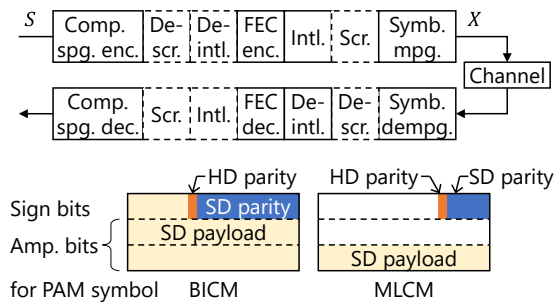

**Fig. 1:** System model (top) and frame structure (bottom).

is the channel-input symbol entropy $\mathbb{H}(X)$ in compressed shaping systems, where the conventional bit scrambling, which influences the amplitudes of channel-input symbols, is omitted.

We have recently compared the transmission performance in [10] between bit-interleaved coded modulation (BICM) [11] and multilevel coded modulation (MLCM) [12], without compressed shaping. In either case, the FEC consists of an inner SD-FEC with code rate 4/5 and an outer hard-decision (HD) FEC with code rate 0.9922 [13]. A DVB-S2 low-density parity check code [14] with codeword length 64800 and a maximum of 20 decoding iterations was used for the SD-FEC. In the MLCM, the least significant bit tributary for the pulse amplitude modulation (PAM) symbols is protected by the SD-FEC, and the parity bits are placed at the sign bit tributary. All bits are protected by the outer HD-FEC code.

The amplitudes of X are given by the compressed shaping encoder, based on hierarchical distribution matching [15], having a dual-polarized in-phase and quadrature four-dimensional block length of 128 with 424 input bits. The source's mark ratio deviation from the default value of 0.5, ΔP_S was swept from 0 to 0.45. For comparison, uniform QAM was also examined. Compared with uniform BIC-64-QAM, compressively shaped MLC-64-QAM has the

Tab. 1: Statistics of channel-input symbols in compressively shaped 64-QAM.

ΔP_S	0	0.1	0.2	0.3	0.4	0.45
$\mathbb{H}(S)$	1	0.9710	0.8813	0.7219	0.4690	0.2864
$P_A(1)$	0.4514	0.4706	0.5013	0.5561	0.6729	0.7892
$P_A(3)$	0.3326	0.3258	0.3108	0.2786	0.2055	0.1320
$P_A(5)$	0.1659	0.1576	0.1465	0.1298	0.0967	0.0633
$P_A(7)$	0.0500	0.0460	0.0414	0.0355	0.0249	0.0154
$\mathbb{H}(A)$	1.692	1.663	1.620	1.538	1.312	1.000
G [dB]	1.091	1.290	1.573	2.055	3.214	4.759
PAPR [dB]	3.872	4.071	3.354	4.836	5.995	7.540
Ex. kurtosis	−0.291	−0.242	−0.164	−0.007	0.454	1.192

Fig. 2: Channel-output constellations.
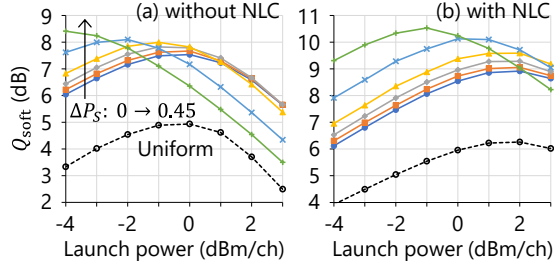
Fig. 3: Transmission performance for compressively shaped BIC-64-QAM (a) without or (b) with NLC.

Fig. 4: Transmission performance for compressively shaped MLC-64-QAM (a) without or (b) with NLC.

same information rate (~4.76 bits per channel use) and a smaller SD-FEC throughput (5/12).

Root-raised cosine (RRC) lowpass filtering was applied with a roll-off factor of 10%. The symbol rate was 32 Gbaud including pilot signals. Any transmitter imperfections were emulated by loading AWGN with an SNR of 25 dB. Eleven wavelength channels were multiplexed at a frequency spacing of 50 GHz, where the center wavelength was the channel under test. The transmission line consisted of 8 or 12 spans of 80 km standard single-mode fiber and intermediate optical nodes with a point-to-point architecture. The fiber parameters were: a loss coefficient of 0.2 dB/km, a local chromatic dispersion (CD) of 17 ps/nm/km, and a nonlinear coefficient of 1.3 /W/km. The loss was compensated in each node by erbium-doped fiber amplifiers, having a noise figure of 8 dB per node. Laser phase noise and polarization-related impairments were neglected. The fiber propagation was numerically simulated by the split-step Fourier method. Each wavelength channel was coherently detected and fed to the DSP chain.

Firstly, we performed either linear equalization for CD compensation (CDC) or NLC including CDC. For the NLC, we used multi-channel LDBP at 1 step/span, addressing nonlinear waveform distortion due to self- and cross-phase modulation [9]. Several parameters at each span such as fiber dispersion, nonlinearity, and walkoff between the channels were optimized by the stochastic gradient descent algorithm. As a result, the optimized parameters at 1 step/span could be different from the given physical values, leading to a better NLC

performance than single-channel DBP at 2 step/span.

Subsequently, the channel-output symbols X were extracted by RRC matched filtering and pilot-aided carrier recovery, assuming a fixed phase rotation during each simulation batch. The channel-output symbols were softly demapped to logarithmic ratios of *a posteriori* probabilities (L-values), followed by SD-FEC decoding.

Transmission and FEC simulations are decoupled by employing a virtual (de)scrambler and (de)interleaver for efficient evaluations [16]. The (de)interleaver outside the FEC coding also serves to maintain the time-order of a symbol sequence, improving the nonlinearity tolerance with short block lengths [16,17].

Simulation results

The channel-input symbol statistics, soft Q-factor Q_{soft} of the SD-FEC decoder input [18], and relative power consumption in the SD-FEC decoder were evaluated by simulations. Tab. 1 summarizes the statistics of source bits and channel-input symbols, i.e., source and channel-
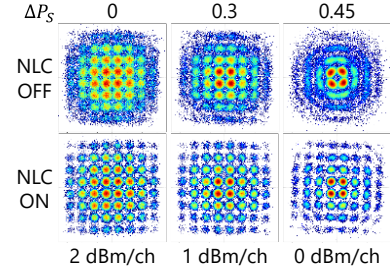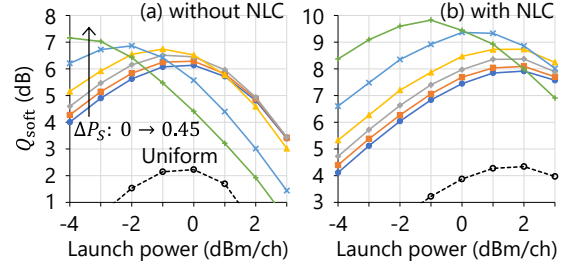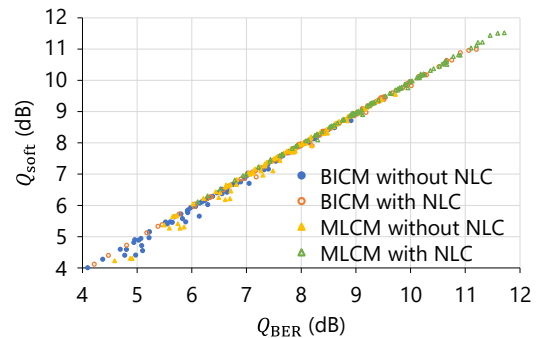
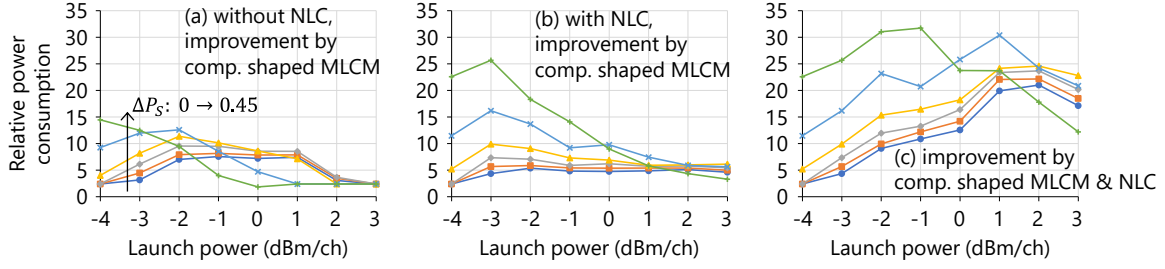**Fig. 5:** Comparison of soft and hard Q-factors.

Fig. 6: Relative SD-FEC decoding power consumption: (a) and (b) shows improvement by compressed shaping and MLCM under (a) without or (b) with NLC, while (c) does improvement by both compressed shaping and NLC.

input entropies $\mathbb{H}(S)$ and $\mathbb{H}(A)$, probability mass function $P_A(a)$ of the one-dimensional amplitude A, where $a \in \{1,3,5,7\}$, constellation gain $G = d_{\min}^2(2^\beta - 1)/(6E)$, and excess kurtosis $\mathbb{E}[|X|^4]/\mathbb{E}^2[|X|^2] - 2$. Here, $d_{\min}(=2)$, E, β, and $\mathbb{E}[\cdot]$ denote the minimum Euclidean distance, the average symbol energy, the spectral efficiency, and an expectation, respectively. A higher G results in not only lower required SNR for AWGN channels but also higher peak-to-average power ratio (PAPR) and excess kurtosis at the channel input. Then, fiber nonlinearity degrades the received constellations, as shown in Fig. 2.

Figs. 3 and 4 show Q_{soft} after 12-span transmission as a function of launch power for compressively-shaped 64-QAM in BICM and MLCM schemes, respectively. In the linear regime such as at –4 dBm/ch, Q_{soft} increases with increasing ΔP_S, while it decreases with increasing ΔP_S in the highly nonlinear regime, e.g., at +2 dBm/ch without NLC (Figs. 3(a) and 4(a)). The nonlinear degradation is particularly severe if $\Delta P_S \geq 0.1$ in the examined cases. The optimum launch power, providing the highest Q_{soft}, decreases by 1, 2, or ~4 dB for ΔP_S=0.3, 0.4, or 0.45, respectively. The reduced launch power originates from the increased channel-input PAPR and excess kurtosis. Stopping the compression at $\Delta P_S \leq 0.3$ or maintaining the peak launch power (i.e., reducing the average launch power according to the channel-input PAPR) by adjusting the gain in DSP or optoelectronic devices can reduce the degradation. For example, by setting the default launch power to 0 dBm/ch for ΔP_S=0, the launch power for ΔP_S=0.45 is shifted to –3.7 dBm/ch by the difference of the channel-input PAPR. In Figs. 3(b) and 4(b), NLC recovered most of the excess nonlinear degradations, and optimum launch powers were 2–3 dB larger than without NLC.

The soft Q-factor Q_{soft} takes soft information into account and is a reliable performance metric, benchmarking the BER after SD-FEC decoding better than the conventional (hard) Q-factor Q_{BER}, which is computed from the pre-SD-FEC BER. Fig. 5 compares these Q-factors for BICM or

MLCM with 8 or 12 spans. Q_{soft} is correlated with Q_{BER} and 0.5–1 dB less in the low Q regime, which corresponds to cases with small $\mathbb{H}(S)$ and high launch power, without NLC. Subsequently, the SD-FEC decoding power consumption was compared with uniform BIC-64-QAM. The power consumption is assumed to be proportional to the SD-FEC throughput and the average number of decoding iterations [10,12]. The improved power consumption is depicted in Fig. 6. Here, Figs. 6(a) and 6(b) show the improvements by compressed shaping without and with NLC, while Fig. 6(c) applies both compressed shaping and NLC. The maximum improvements were 14, 26, or 32 times in case (a), (b), or (c), respectively, although the additional power consumption for NLC must be considered in cases (b) and (c).

Conclusions and potential future works

In optical fiber transmission of compressively shaped signals, we found that the optimal launch power decreases with source entropy; however, the maximum Q-factor increases. The overall behavior is similar for BICM and MLCM. NLC improves the optimum launch power and the maximum Q-factor by 2–3 dB.

We found severe nonlinearity degradation for signals with high PAPR and excess kurtosis at the channel input, caused by a small source entropy. However, channel-input PAPR and excess kurtosis usually do not influence the transmission performance in CD-uncompensated multi-span transmissions. Potential future works include analyzing the time evolution of amplitude variations [17,19–21] or non-ideal DSP for understanding the degradation mechanisms.

References

[1] K. Roberts, M. O'Sullivan, K.-T. Wu, H. Sun, A. Awadalla, D. J. Krause, and C. Laperle, "Performance of dual-polarization QPSK for optical transport systems," J. Lightw. Technol., vol. 27, no. 16, pp. 3546–3559, Aug. 2009, doi: 10.1109/JLT.2009.2022484.

[2] J. M. Gené, X. Chen, J. Cho, S. Chandrasekhar, and P. Winzer, "Experimental demonstration of widely tunable rate/reach adaptation from 80 km to 12,000 km using probabilistic constellation shaping," in Proc. Opt. Fib. Commun. Conf. (OFC), San Diego, CA, USA, Mar. 2020, Paper M3G.3, doi: 10.1364/OFC.2020.M3G.3.

[3] 400ZR, [Online]. Available: https://www.oiforum.com/technical-work/hot-topics/400zr-2

[4] Open ROADM MSA, [Online]. Available: www.openroadm.org/home.html

[5] G. Böcherer, F. Steiner, and P. Schulte, "Bandwidth efficient and rate-matched low-density parity-check coded modulation," IEEE Trans. Commun., vol. 63, no. 12, pp. 4651-4665, Dec. 2015 , doi: 10.1109/TCOMM.2015.2494016.

[6] F. Buchali, F. Steiner, G. Böcherer, L. Schmalen, P. Schulte, and W. Idler, "Rate adaptation and reach increase by probabilistically shaped 64-QAM: an experimental demonstration," J. Lightw. Technol., vol. 34, no. 7, pp. 1599-1609, Apr. 2016 , doi: 10.1109/JLT.2015.2510034.

[7] T. Yoshida, M. Karlsson, and E. Agrell, "Joint source–channel coding via compressed distribution matching in fiber-optic communications," Proc. Opt. Fib. Commun. Conf. (OFC), San Diego, CA, USA, Mar. 2019, Paper M4B.6, doi: 10.1364/OFC.2019.M4B.6.

[8] T. Yoshida, K. Igarashi, M. Karlsson, and E. Agrell, "Compressed shaping: concept and FPGA demonstration," J. Lightw. Technol., vol. 39, no. 17, pp. 5412–5422, Sep. 2021, doi: 10.1109/JLT.2021.3085974.

[9] T. Inoue, R. Matsumoto, and S. Namiki, "Learning-based digital back propagation to compensate for fiber nonlinearity considering self-phase and cross-phase modulation for wavelength-division multiplexed systems," Opt. Express, vol. 39, no. 9, pp. 14851–14872, Apr. 2022, doi: 10.1364/OE.454841.

[10] T. Yoshida, T. Inoue, M. Binkai, K. Matsuda, S. Koshikawa, Y. Konishi, and N. Suzuki, "Interplay of probabilistically shaped multilevel coded modulation and fiber nonlinearity compensation," OptoElectronics Commun. Conf. (OECC), Toyama, Japan, July 2022, to appear.

[11] G. Caire, G. Taricco, and E. Biglieri, "Bit-interleaved coded modulation," IEEE Trans. Inf. Theory, vol. 44, no. 3, pp. 927-946, May 1998, doi: 10.1109/18.669123.

[12] T. Yoshida, M. Karlsson, and E. Agrell, "Multilevel coding with flexible probabilistic shaping for rate-adaptive and low-power optical communications," in Proc. Opt. Fib. Commun. Conf. (OFC), San Diego, CA, USA, Mar. 2020, Paper M3J.7, doi: 10.1364/OFC.2020.M3J.7.

[13] D. S. Millar, R. Maher, D. Lavery, T. Koike-Akino, M. Pajovic, A. Alvarado, M. Paskov, K. Kojima, K. Parsons, B. C. Thomsen, S. J. Savory, and P. Bayvel, "Detection of a 1 Tb/s superchannel with a single coherent receiver," in Proc. Eur. Conf. Opt. Commun. (ECOC), Valencia, Spain, Sep.-Oct. 2015, Paper Mo.3.3.1, doi: 10.1109/ECOC.2015.7341618.

[14] European Telecommunications Standards Institute, Second generation framing structure, channel coding and modulation systems for broadcasting, interactive services, news gathering and other broadband satellite applications; Part 1 (DVB-S2), ETSI Standard EN 302 307-1 V1.4.1, Nov. 2014. [Online]. Available: www.dvb.org/standards

[15] T. Yoshida, M. Karlsson, and E. Agrell, "Hierarchical distribution matching for probabilistically shaped coded modulation," J. Lightw. Technol., vol. 37, no. 6, pp. 1579–1589, Mar. 2019, doi: 10.1109/JLT.2019.2895065.

[16] T. Yoshida, M. Karlsson, E. Agrell, "Efficient offline evaluation of FEC codes based on captured data with probabilistic shaping," in Proc. Opt. Fib. Commun. Conf. (OFC), San Diego, CA, USA, Mar. 2018, Paper M4E.5, doi: 10.1364/OFC.2018.M4E.5.

[17] W.-R. Peng, A. Li, Q. Guo, Y. Cui, and Y. Bai, "Transmission method of improved fiber nonlinearity tolerance for probabilistic amplitude shaping," Opt. Express, vol. 28, no. 20, pp. 29430–29441, Sep. 2020, doi: 10.1364/OE.400549.

[18] E. Agrell, M. Secondini, A. Alvarado, and T. Yoshida, "Performance prediction recipes for optical links," IEEE Photon. Technol. Lett., vol. 33, no. 18, pp. 1034–1037, Sep. 2021, doi: 10.1109/LPT.2021.3093790.

[19] A. Amari, S. Goossens, Y. C. Gültekin, O. Vassilieva, I. Kim, T. Ikeuchi, C. M. Okonkwo, F. M. J. Willems, and A. Alvarado, "Introducing enumerative sphere shaping for optical communication systems with short blocklengths," in Journal of Lightwave Technology, vol. 37, no. 23, pp. 5926–5936, Dec. 2019, doi: 10.1109/JLT.2019.2943938.

[20] K. Wu, G. Liga, A. Sheikh, F. M. J. Willems, and A. Alvarado, "Temporal energy analysis of symbol sequences for fiber nonlinear interference modelling via energy dispersion index," J. Lightw. Technol., vol. 39, no. 18, pp. 5766–5782, Sep. 2021, doi: 10.1109/JLT.2021.3092176.

[21] J. Cho and R. Tkach, "On the Kurtosis of Modulation Formats for Characterizing the Nonlinear Fiber Propagation," J. Lightw. Technol., preprint, doi: 10.1109/JLT.2022.3152411.